Available online at www.sciencedirect.com
ScienceDirect
Journal of Solid State Chemistry 180 (2007) 2080–2087
JOURNAL OF SOLID STATE CHEMISTRY
www.elsevier.com/locate/jssc

Vapor-thermal preparation of highly crystallized TiO_2 powder and its photocatalytic activity

Yaorong Su[a], Jiaguo Yu[a,*], Jun Lin[b,**]

[a]*State Key Laboratory of Advanced Technology for Material Synthesis and Processing, Wuhan University of Technology, Luoshi Road 122#, Wuhan 430070, PR China*

[b]*Department of Chemistry, Renmin University of China, Beijing 100872, PR China*

Received 10 January 2007; received in revised form 4 April 2007; accepted 20 April 2007
Available online 21 May 2007

Abstract

Nanocrystalline anatase TiO_2 powder photocatalysts were synthesized by a vapor-thermal method using tetrabutyl titanate as precursor at a temperature range from 120 to 200 °C. The as-synthesized products were characterized by X-ray diffraction, N_2 adsorption–desorption measurement, transmission electron microscopy, high resolution transmission electron microscopy, Fourier transform infrared spectra, Raman spectra, and their photocatalytic activity was evaluated by photocatalytic oxidation decomposition of acetone in air. The results showed that reaction temperature greatly affected the microstructures and photocatalytic activity of the samples. With increasing reaction temperature and time, the average crystalline size of TiO_2 particles increased and their crystallization enhanced, while the specific surface area of the products decreased. The TiO_2 powders obtained at a temperature range from 150 to 200 °C for 10 h showed good photocatalytic activity and were greatly higher than that of Degussa P-25.

Keywords: Titania; Vapor thermal; Photocatalytic activity; Mesoporous; Nanocrystalline

1. Introduction

In recent 10 years, a great deal of effort has been devoted to developing heterogeneous semiconductor photocatalysts with high photocatalytic activities for their wide environmental applications such as air purification, water disinfection, hazardous waste remediation and water purification [1–15]. Among various oxide semiconductor photocatalysts, titanium dioxide has been proved to be one of the best photocatalysts due to its biological and chemical inertness, strong oxidizing power, cost-effectiveness and long-term stability against photocorrosion and chemical corrosion for widespread environmental applications. However, the photocatalytic activity of titania must be further enhanced from the point of view of practical use and commerce. To achieve this purpose, the prepared anatase TiO_2 powders with good crystallization, small crystallite size, mesoporous structures and high specific surface area are prerequisite to enhance the photocatalytic activity [10,12,13]. There are many methods available for the synthesis of nano-sized TiO_2 powder photocatalyst, such as, ultrasonic irradiation [4], UV light assistance [10], solvent evaporation-induced crystallization [12,13], sol–gel [11], hydrothermal [14,15] and so on. Among these methods, the sol–gel method was most widely used due to its inexpensive equipment required, low temperatures and the homogeneous and highly pure product produced. Usually, the products obtained by this method are amorphous in nature and calcination temperature higher than 350 °C are required to realize the phase transition form amorphous to anatase [10,11]. However, such high calcination temperatures would result in the aggregation and growth of nanocrystalline particles and the rapid decrease of specific surface area. To obtain small nanocrystalline TiO_2 powders with high specific surface area, a reasonable pathway would be to lower thermal-treatment temperature of the phase transition. Hydrolysis of titanium

*Corresponding author.
**Also corresponding author.
E-mail addresses: jiaguoyu@yahoo.com (J. Yu), jlin@chem.ruc.edu.cn (J. Lin).

0022-4596/$ - see front matter © 2007 Elsevier Inc. All rights reserved.
doi:10.1016/j.jssc.2007.04.028

precursor with water vapor is a newly developed method to synthesize nano-sized titanium dioxide [16,17], and the prepared TiO_2 samples exhibit high photocatalytic activity due to their large specific surface area and high crystallinity [18,19]. In this paper, we describe an efficient vapor-thermal method for preparing highly photoactive nano-sized TiO_2 photocatalyst by hydrolysis of tetrabutyl titanate (TBOT) with water vapor at a temperature range from 120 to 200 °C.

2. Experimental

2.1. Preparation

To prepare nanocrystalline TiO_2 powders, TBOT was used as titanium source. Experimental apparatus of vapor-thermal reaction is shown in Fig. 1. The detailed vapor-thermal process was as follows: 15 ml TBOT was placed into a 50 ml Teflon liner, which was then placed into a 200 ml stainless steel autoclave with a Teflon liner. In the gap between the two liner walls, 40 ml of distilled water was added. At the beginning, distilled water did not contact with TBOT. After seal, the autoclave was heated to a desired temperature range (120–200 °C) and kept at that temperature for different time (1–48 h). During the reaction, distilled water in the gap would vaporize. The water vapor came into contact with TBOT and then result in the hydrolyzation of TBOT. After the autoclave was cooled to room temperature, the supernatant was decanted and the resulting precipitates were washed repeatedly with distilled water, and then dried at 80 °C in a vacuum oven for 10 h and finally ground to fine powders with an agate mortar.

2.2. Characterization

The X-ray diffraction (XRD) patterns obtained on an X-ray diffractometer (type HZG41B-PC) using Cu Kα radiation at a scan rate of 0.05° $2\theta\,s^{-1}$ were used to determine the identity of the phase present and crystallite sizes of the TiO_2 powders. The average crystallite sizes of anatase were determined by the Scherrer equation using the FWHM (full width at the half maximum) data of anatase phase after correcting the instrumental broadening [20–22]. The Brunauer–Emmett–Teller (BET) surface area (S_{BET}) of the powders was analyzed by nitrogen adsorption using a Micromeritics ASAP 2020 nitrogen adsorption apparatus (USA). The as-prepared samples were degassed at 100 °C prior to nitrogen adsorption measurements. The BET surface area was determined by a multipoint BET method using the adsorption data in the relative pressure (P/P_0) range of 0.05–0.3. Desorption isotherm was used to determine the pore size distribution using the Barret–Joyner–Halender (BJH) method [23]. The nitrogen adsorption volume at the relative pressure (P/P_0) of 0.994 was used to determine the pore volume and average pore size. Crystallite sizes and shapes were observed using transmission electron microscopy (TEM) and high-resolution transmission electron microscopy (HRTEM) (JEOL-2010F at 200 kV). The samples for TEM observation were prepared by dispersing the TiO_2 powders in an absolute ethanol under ultrasonic irradiation; the dispersion was then dropped on carbon-coated copper grids. Fourier transform infrared (FTIR) spectra on pellets of the samples mixed with KBr were recorded on a Nicolet Magna 560 FTIR spectrometer at a resolution of $4\,cm^{-1}$. The concentration of the samples was kept at about 0.25–0.3%. Raman spectra were recorded at room temperature using a micro-Raman spectrometer (Renishaw InVia) with a 514.5 nm Ar^+ laser as the excitation source in a backscattering geometry. The incident laser power on the samples was less than 10 mW.

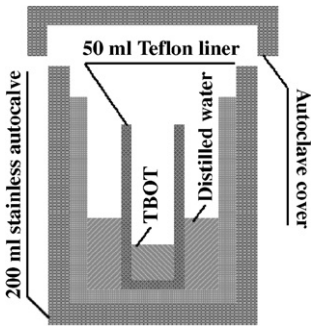

Fig. 1. Illustration of reaction apparatus.

2.3. Measurement of photocatalytic activity

Acetone, formaldehyde and other volatile organic compounds (VOCs) are common indoor air pollutants in modern houses, which have been the subject of numerous complaints regarding health disorders, such as leukemia, nausea, headache and fatigue. These volatile harmful gases usually come from the plywood, particleboard and adhesives for wall clothes, which have been used in construction and furnishing. In order to improve indoor air quality (IAQ), these volatile organic compounds (VOCs) must be eliminated. Therefore, we chose acetone as a model contaminate chemical to characterize the photocatalytic activity of the prepared samples. The photocatalytic oxidation of acetone in air is based on the following reaction [24,25]:

$$CH_3COCH_3 + 4\,O_2 \rightarrow 3\,CO_2 + 3\,H_2O. \quad (1)$$

The photocatalytic activity measurements of the as-prepared TiO_2 powders and Degussa P-25 for the oxidation of acetone in air were performed at room temperature using a 15 L photocatalytic reactor, followed by the photodegradation of acetone with an initial concentration of 400 ± 20 ppm. The detailed experimental setup and process were reported elsewhere [24]. The weight of the TiO_2 catalysts used for each experiment was kept at 0.3 g. After the catalysts were placed in the reactor, a small amount of acetone was injected with a syringe. The acetone vapor was allowed to reach adsorption–desorption

equilibrium with catalysts in the reactor prior to UV light irradiation. A 15 W 365 nm UV lamp was used as light source and its intensity striking on the coating measured with a UV radiometer (Model: UV-A, made in Photoelectric Instrument Factory of Beijing Normal University) was 2.5 mW/cm^2. The concentration analysis of acetone, carbon dioxide, and water vapor in the reaction was conducted on line with a Photoacoustic IR Multigas Monitor (INNOVA Air Tech Instruments Model 1312). Each set of experiment was followed for 60 min.The photocatalytic activity of the TiO_2 samples can be quantitatively evaluated by comparing the apparent reaction rate constants. The photocatalytic oxidation of acetone is a pseudo-first-order reaction and its kinetics may be expressed as follows: $\ln(C_0/C) = kt$ [24], where k is the apparent reaction rate constant, C_0 and C are the initial concentration and the reaction concentration of acetone, respectively. The photocatalytic activity of Degussa P-25 (P25) powders was also measured as a reference.

3. Results and discussion

3.1. Crystal structure

XRD was used to characterize the phase structure of the as-prepared samples. The XRD patterns and related physical properties of the TiO_2 samples prepared at different temperatures and time are shown in Figs. 2, 3 and Table 1. It can be seen from Fig. 2 that all diffraction peaks can be easily indexed to a pure anatase phase of TiO_2 (JCPDS No. 21-1272, space group: $I4_1/amd$ (1 4 1)). With increasing reaction temperatures, the peak intensities of anatase phase increase, while the widths of the (1 0 1) diffraction peak of anatase become narrower, indicating enhancement of crystallization and formation of larger

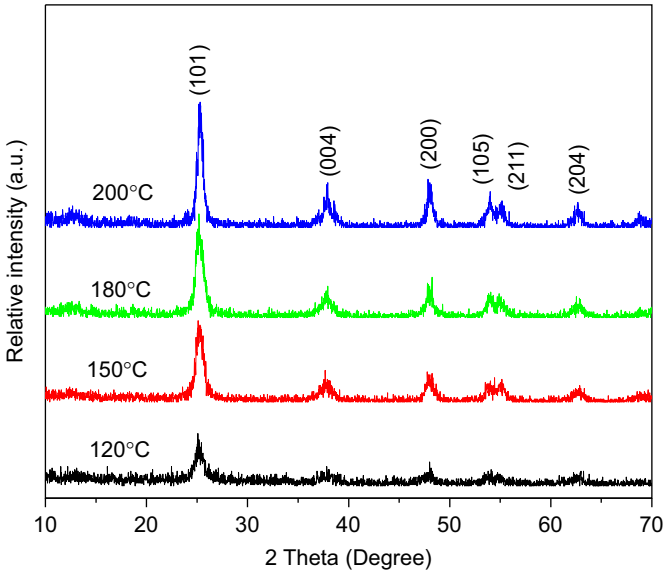

Fig. 2. XRD patterns of the TiO_2 samples prepared at different temperatures for 10 h.

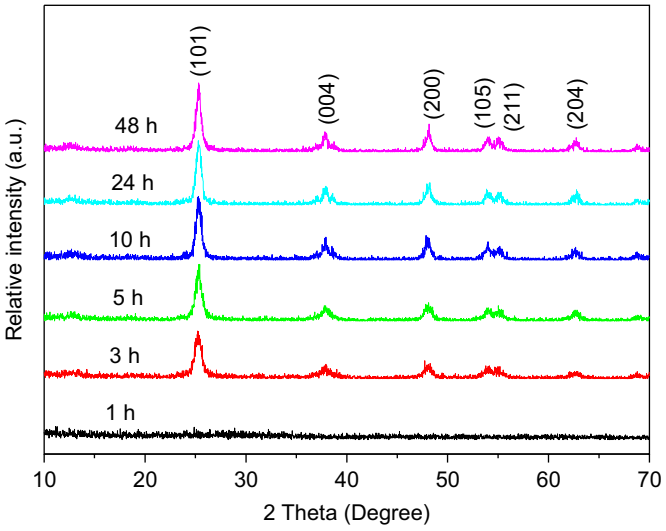

Fig. 3. XRD patterns of the TiO_2 samples prepared at 200 °C for different reaction time.

crystallites. Further investigation shows that reaction time also obviously influence the crystallization of TiO_2 (see Fig. 3). When reaction temperature is kept at 200 °C, at 1 h, no diffraction peaks are observed (Fig. 3), indicating that the prepared products are amorphous. At 3 h, the diffraction peaks of anatase begin to appear (Fig. 3), suggesting that the crystallization occurs at 200 °C for 3 h. With further prolonging the reaction time, the intensities of XRD peaks of anatase phase increase, indicating enhancement of crystallization. The crystallite size of all TiO_2 powders calculated according to Scherrer equation using the FWHM data of the (1 0 1) peak are summarized in Table 1. It can be seen that the crystallite size of the obtained TiO_2 powders increases with increasing reaction temperature and time.

3.2. BET surface areas and pore structure

Fig. 4 shows the nitrogen adsorption–desorption isotherms of the samples prepared at different temperatures for 10 h. At 120 °C, the isotherms are a combination of type I and IV (BDDT classification), and have two small hysteresis loops, implying that the sample contains micropores and mesopores, and has a bimodal pore size distribution in the mesoporous region. Moreover, the shapes of the two hysteresis loops are different from each other. At a low relative pressure from 0.4 to 0.8, the hysteresis loop is of type H2, indicating the pores with narrow necks and wider bodies (ink-bottle pores) [23,26]. However, at higher relative pressure from 0.8 to 1.0, the shape of the hysteresis loop is of type H3, associated with aggregates with narrow slit-like pores [23,26]. At high temperatures (150, 180 and 200 °C), the prepared samples have type IV isotherms and type H3 hysteresis loops, suggesting that the powders are mesoporous structures and the pores appear narrow slit-shaped shapes, indicating that the prepared particles are plate-like particles [23].

Table 1
Effects of preparation temperatures and time on physical properties of TiO_2 samples[a]

Temp. (°C)	Time (h)	S_{BET}[b] (m^2/g)	Pore volume[c] (cm^3/g)	Average pore[d] size (nm)	Porosity[e] (%)	Crystalline[f] size (nm)
120	10	250.4	0.177	2.82	40.8	7.6(1.00)
150	10	140.7	0.278	7.90	52.1	9.6(1.62)
180	10	119.6	0.358	12.0	58.3	10.1(2.12)
200	10	92.5	0.365	15.8	58.8	12.7(2.54)
200	1	253.3	0.125	1.97	32.8	/
200	3	121.4	0.162	5.34	38.8	9.9(2.13)
200	5	118.7	0.284	9.56	52.6	11.2(2.25)
200	24	89.4	0.339	15.2	57.0	13.0(2.74)
200	48	71.2	0.270	15.1	51.3	14.8(2.99)

Relative anatase crystallinity: the relative intensity of the diffraction peak from the anatase (1 0 1) plane (indicated in parentheses, reference sample prepared at 120 °C for 10 h).

[a]All samples listed in Table 1 are anatase phase.

[b]BET surface area calculated from the linear part of the adsorption isotherm ($P/P_0 = 0.05$–0.3).

[c]Total pore volume, taken from the volume of N_2 adsorbed at $P/P_0 = 0.994$.

[d]Average pore diameter, estimated using the desorption branch of the isotherm and the Barrett–Joyner–Halenda (BJH) method.

[e]The porosity is estimated from the pore volume determined using the adsorption branch of the N_2 isotherm at $P/P_0 = 0.994$.

[f]The average crystalline size of TiO_2 was calculated by XRD using the Scherrer equation.

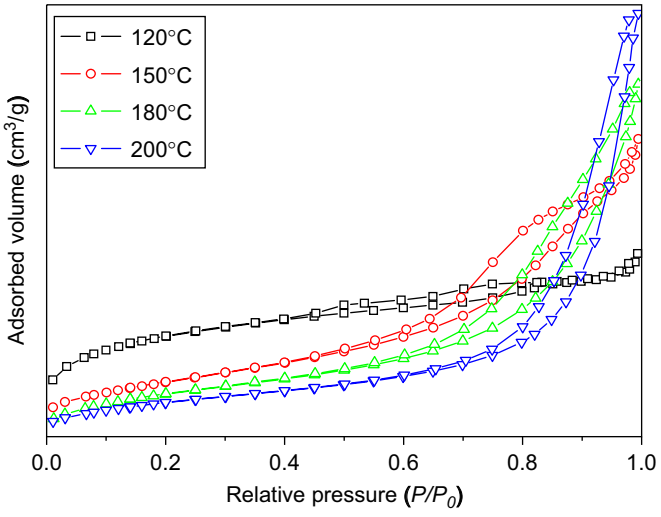

Fig. 4. Nitrogen adsorption–desorption isotherms of the TiO_2 samples prepared at different temperatures for 10 h.

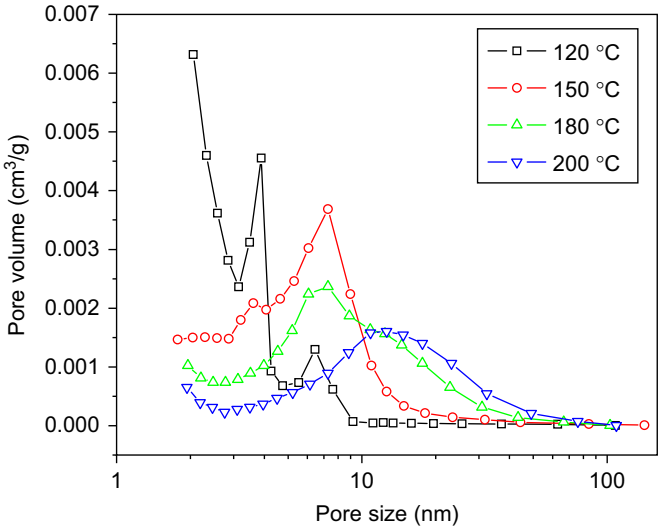

Fig. 5. Pore size distribution curves of the TiO_2 samples prepared at different temperatures for 10 h.

Fig. 5 shows the corresponding pore size distribution of the samples prepared at different temperatures for 10 h. The sample prepared at 120 °C shows a trimodal pore size distribution in the microporous and mesoporous region. There are two kinds of mesopores, and their size located at ca. 3–4 nm and ca. 5–9 nm, respectively, which probably came from aggregation of inter-crystallites. In addition, the sample still contained micropores, which probably came from amorphous titania remained in the sample [27]. With increasing reaction temperatures, the pore size distribution gradually turned into monomodal distributions from trimodal, and the peak pore sizes shift to right. The change in the pore size distributions and the shift of the peak pore sizes may be due to the difference in crystallization (or crystallinity) (see Fig. 2 and Table 1). Table 1 showed that the specific surface area of the samples monotonically decreases with increasing reaction temperature and time, on the contrary, pore size increase due to the crystallite growth [26]. Further observation indicated that the pore volume and porosity also increase with increasing reaction temperature. This may be attributed to the reduction of content of some amorphous titania inserted into the pores of mesopores TiO_2.

3.3. Raman spectroscopy

Raman spectroscopy can provide valuable information on the phase composition, crystallinity, crystallite size, and defect (oxygen vacancy) concentrations of TiO_2. The crystal structure of anatase titanium dioxide is tetragonal

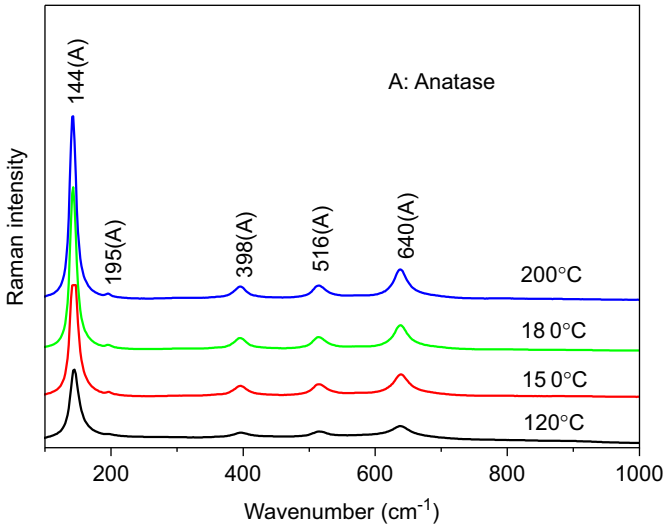

Fig. 6. Raman spectra of the TiO_2 samples prepared at 120, 150, 180 and 200 °C for 10 h.

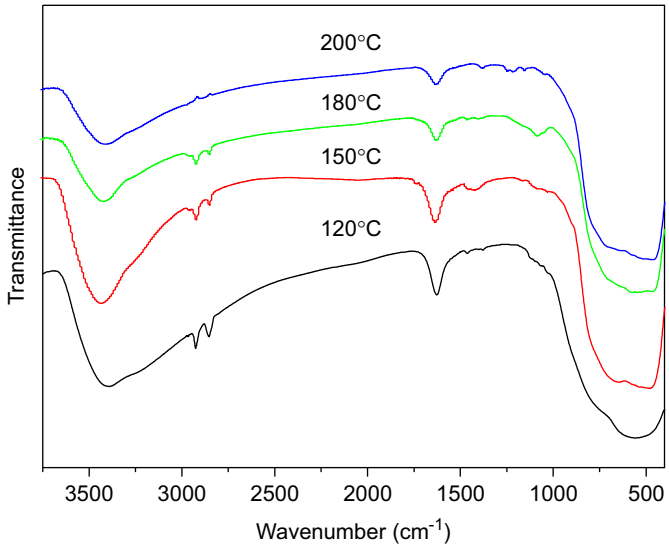

Fig. 7. FTIR spectra of the TiO_2 samples prepared at 120, 150, 180 and 200 °C for 10 h.

with space group D_{4h}^{19} [28]. Factor group analysis indicates that there exist 15 optical modes in the anatase TiO_2 with the irreducible representations, $1A_{1g}+1A_{2u}+1B_{1g}+1B_{2u}+3E_g+2E_u$. Among these modes A_{1g}, B_{1g} and E_g are Raman active and those of A_{2u}, $B_{2u}$and E_u are infrared active [29].

Fig. 6 shows the Raman spectra of the samples prepared at different temperatures for 10 h. In the Raman spectra of the samples, we can observe several characteristic peaks of TiO_2 anatase phase at 144, 195, 398, 516 and 640 cm^{-1}. Based on the factor group analysis, the 398 cm^{-1} peak is assigned to the B_{1g} mode (v_4); 640 cm^{-1} peak can be attributed to the E_g mode (v_1); 516 cm^{-1} peak can be attributed to the $A_{1g}+B_{1g}$ modes (v_2+v_3). The peaks at 195 and 144 cm^{-1} are assigned to the E_g modes represented by v_5 and v_6 [30].

Moreover, there is no significant change in the peak position but the intensity of the peaks increase with increasing the reaction temperature. The FWHM corresponding to the peak at 144 cm^{-1} is found to be 16.7, 15.5, 11.7 and 10.7 cm^{-1} for the samples prepared at temperatures 120, 150, 180 and 200 °C, respectively, indicating a decrease in FWHM with increasing reaction temperature. The increase of intensity of the peaks and the decrease of FWHM can be attributed to the improvement in the crystallinity of the samples [31].

3.4. FTIR spectra

The FTIR spectra of the samples prepared at different temperature for 10 h are shown in Fig. 7. It is believed that the broad peak at 3400 cm^{-1} and the relatively sharp peak at 1650 cm^{-1} correspond to the surface-adsorbed water and hydroxyl groups, respectively. Obviously, with increasing the reaction temperature, the surface-adsorbed water and hydroxyl groups decrease slightly. This can be due to the decrease of specific surface areas and increase of crystallinity (as shown in Table 1). The main peak at 400–700 cm^{-1} is due to Ti–O stretching and Ti–O–Ti bridging stretching modes [26]. Besides, two weak bands at 2924 and 2854 cm^{-1} (ν_{CH} and ν_{CH2}) can be ascribed to the characteristic frequencies of residual organic species, which is not completely removed by distilled water washing [32]. Further observation indicates that the intensities of these peaks decrease with increasing the reaction temperatures, suggesting that the amount of residual organic species decreases gradually. This might be due to the fact that most of organic moieties were eliminated from the product during the vapor-thermal synthesis at higher temperature. The small peaks at 1380-1400 cm^{-1} region could be ascribed to carboxyl (C = O) groups [33], which might have resulted from the oxidation of the organic species during the vapor-thermal treatment.

3.5. TEM study

Fig. 8 shows the TEM and HRTEM images of the TiO_2 sample prepared at 200 °C for 10 h. It can be seen that the particles appear a relatively uniform size distribution (Fig. 8a and b). The mesoporous structures in powders could be observed from TEM image (Fig. 8a and b) due to the aggregates of the particles. According to previous results of nitrogen adsorption and desorption isotherms, the type H3 loop is observed with aggregates of plate-like particles giving rise to slit-shaped pores, implying that the prepared particles are plate-like particles. The average size of the primary particles estimated from the TEM image is about 12 ± 1 nm, which is in good agreement with that calculated from the XRD pattern using Scherrer equation (12.7 nm) (as shown in Table 1). HRTEM image (Fig. 8c) clearly indicates that the as-prepared TiO_2 particles are highly crystallized and a set of clear lattice fringes are

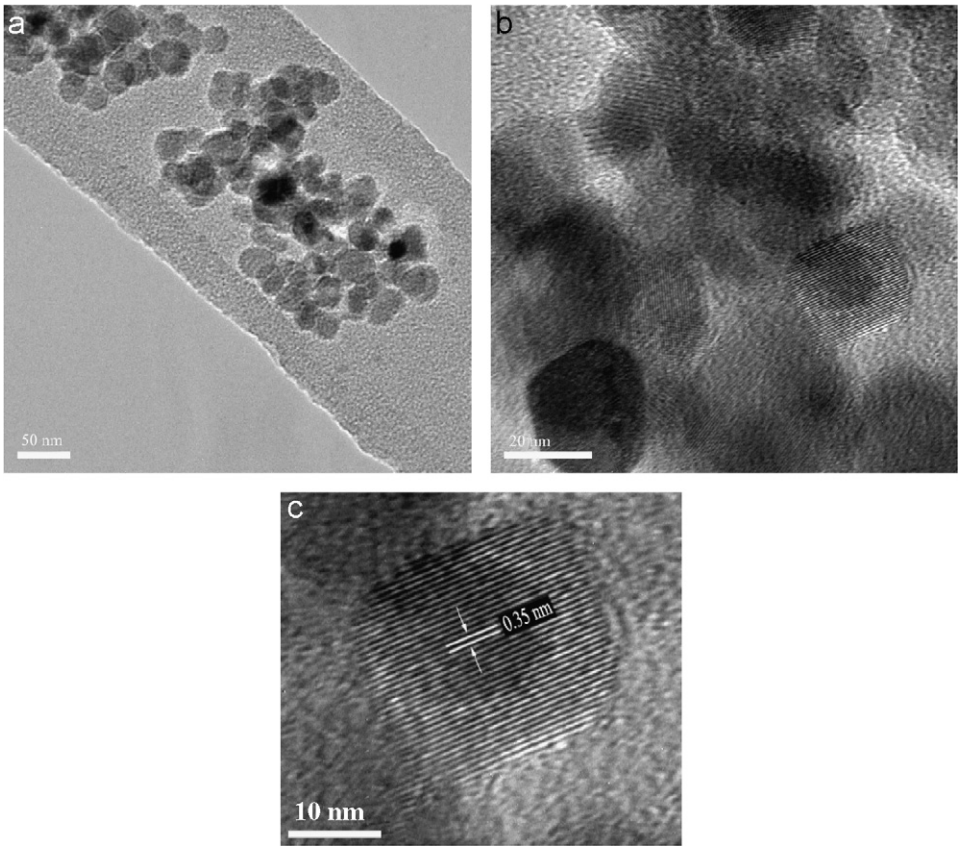

Fig. 8. TEM (a) and HRTEM (b) and (c) images of the TiO_2 powders prepared at 200 °C for 10 h.

present throughout the particle, giving additional evidence that the particles are highly crystallized. The distance between the fringes is 0.35 nm, agrees well with that of the (1 0 1) crystallographic plane of anatase TiO_2 [14].

3.6. Photocatalytic activity

Fig. 9 shows the effects of reaction temperatures on the photocatalytic activity of the TiO_2 powders prepared under UV irradiation. For the TiO_2 samples prepared at 120 °C, they possess large specific surface area, but show the lowest photocatalytic activity. This is assigned to the fact that the TiO_2 powders prepared at 120 °C have weak crystallization and may contain amorphous phase. As the reaction temperature reaches 150 °C, the photocatalytic activity increased remarkably. With further increase in the reaction temperature, the photocatalytic activity slightly increases. At 200 °C, the as-prepared powders show the highest photocatalytic activity, and their photocatalytic activity are obviously higher than that of P25, which is well known for its high photocatalytic activity. The calculated apparent rate constants of the samples prepared at 120, 150, 180 and 200 °C are 2.91, 10.17, 11.35 and $13.97 \times 10^{-3}\,min^{-1}$, respectively, and the corresponding apparent rate constant for P25 is $3.03 \times 10^{-3}\,min^{-1}$. The photocatalytic activity of TiO_2 powders prepared by this method above 150 °C for 10 h exceeded that of P25, which may be attributed to the

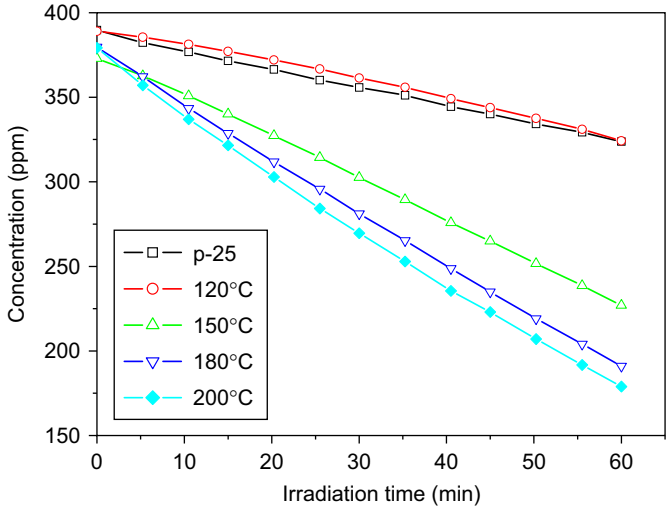

Fig. 9. Reduction of acetone concentration as a function of UV irradiation time in the presence of TiO_2 photocatalysts prepared at different temperatures for 10 h and P25.

fact that these nanocrystalline TiO_2 powders have larger specific surface area, smaller crystallite size and higher purity and so on. The specific surface area and crystallite size of P25 are about 50 m^2/g and 30 nm, respectively.

Much effort has been devoted to understanding the effect of specific surface area on the photocatalytic activity

of a photocatalyst. It is believed that a high specific surface area usually results in high photocatalytic activity due to the fact that the photocatalytic reactions mainly conduct on the illuminated surface. The adsorption on the catalyst surface would be benefit to concentrating the reactant molecules for the photoreactions and the UV light might be scattered by the nano-sized TiO_2 particles. Also, photogenerated electrons and holes as well as the adsorbed molecules might be able to diffuse more or less at the catalyst surface, causing the photoreactions more easily to happen. However, in our experiment, the photocatalytic activity of the samples increases with decreasing specific surface area. The enhancement of the photocatalytic activity is mainly ascribed to two aspects: On one hand, it has been documented that an increase in the crystallization degree of anatase TiO_2 can lead to an enhancement in its catalytic activity for the photocatalytic degradation of organic pollutants in air and wastewater [34–36]. The highly crystallized anatase TiO_2 might have fewer defects that can act as the recombination centers of photogenerated electrons and holes and reduce photocatalytic activity [37,38]. This explanation is valid for the present TiO_2 samples prepared at different temperatures for 10 h. The crystallinity of the TiO_2 sample increases with increasing the reaction temperature, as shown in Table 1. On the other hand, the increase in the photocatalytic activity with increasing the reaction temperature might be due to the increase in pore volume (see Table 1). High pore volume is believed to possess more and greater channels for the diffusion rate of reactants and products. This results in the enhancement of the photoactivity [39].

We also examine the influence of reaction time on the photocatlaytic activity of the TiO_2 samples prepared at 200 °C. The sample prepared at 200 °C for 1 h shows negligible photocatalytic activity due to its amorphous structure (not shown here). The photocatalytic activity of the samples prepared at 200 °C for 3, 5, 10, 24 and 48 h and P25 are shown in Fig. 10. The calculated apparent rate constants of the samples prepared at 200 °C for 3, 5, 10, 24 and 48 h are 2.85, 5.31, 13.97, 6.37 and $5.45 \times 10^{-3}\,min^{-1}$, respectively. The powders prepared at 3 h show relatively low photocatalytic activity due to its weak crystallinity [40]. With increasing the reaction time to 5 h, the photocatalytic activity of the prepared sample obviously increases and is higher than that of P25, which may be due to the fact that the former has larger specific surface area, higher porous volume and smaller crystallite size. The sample prepared at 200 °C for 10 h shows the highest photocatalytic activity. Although the sample prepared at 200 °C for 10 h has larger crystallite size and smaller specific surface area than the sample prepared at 200 °C for 5 h, it possesses better crystallization (see Fig. 3 and Table 1). It has been mentioned above that the photacatalytic cativity also depends on the crystallinity of TiO_2 particles, which strongly influences the recombination rate of the photoexcited electrons (e^-) and holes (h^+). Higher crystallinity, i.e., fewer surface and bulk defects, leads to smaller probability of the recombination of e^-–h^+ and enhances the photocatalytic activity [38]. With further increasing reaction time, the photocatalytic activity decreases, which is assigned to the increase in crystallite size and the decrease in specific surface area and pore volume. According to the above results, it can be inferred that TiO_2 powders with better crystallinity and larger pore volume are expected to be excellent candidates for photocatalytic application.

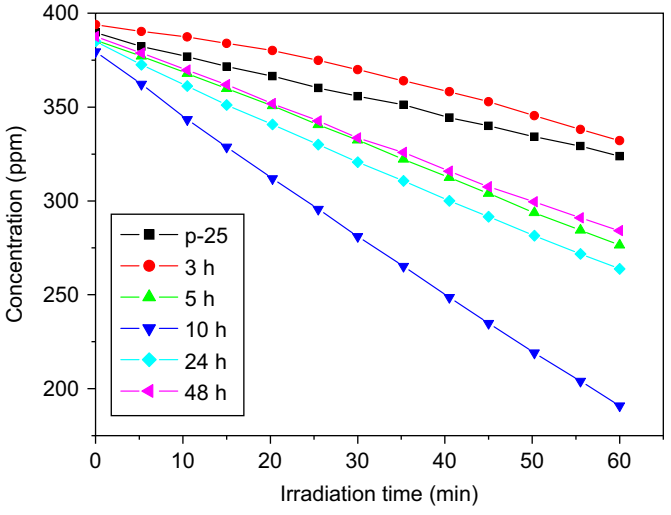

Fig. 10. Reduction of acetone concentration as a function of UV irradiation time in the presence of the samples prepared at 200 °C for different reaction time and P25.

4. Conclusions

Nanocrystalline TiO_2 powders with pure anatase phase were prepared using a vapor-thermal method. The physical properties of the obtained TiO_2 powders, for example, surface area, particle size and pore volume, could be controlled over a wide range by changing the reaction temperature and time. With increasing reaction temperature and time, the crystalline size gradually increased and the specific surface area decreased. The effects of experimental parameters on the photocatalytic activities of the obtained powders were also studied, and it was found that the TiO_2 powders prepared at 200 °C for 10 h showed the highest photocatalytic activity. The high photocatalytic activity of this sample was thought to be due to its better ctystallinity, i.e., fewer crystal defects, giving a slower recombination of photoexcited electrons and positive holes and large pore volume.

Acknowledgments

This work was partially supported by the National Natural Science Foundation of China (20473059 and 50625208). This work was also financially supported by the Key Research Project of Chinese Ministry of Education (No. 106114) and Program for Changjiang Scholars and

Innovative Research Team in University (PCSIRT, No. IRT0547), Ministry of Education, China.

References

[1] C.J.G. Cornu, A.J. Colussi, M.R. Hoffmann, J. Phys. Chem. B 105 (2001) 1351.
[2] A. Fujishima, T.N. Rao, D.A. Tryk, J. Photochem. Photobiol. C 1 (2000) 1.
[3] H. Tada, K. Teranishi, Y. Inubushi, S. Ito, Chem. Commun. 21 (1998) 2345.
[4] J.C. Yu, J.G. Yu, W.K. Ho, L.Z. Zhang, Chem. Commun. (2001) 1942.
[5] M.A. Fox, M.T. Dulay, Chem. Rev. 93 (1993) 341.
[6] J.G. Yu, J.C. Yu, M.K.P. Leung, W.K. Ho, B. Cheng, X.J. Zhao, J.C. Zhao, J. Catal. 217 (2003) 69.
[7] P.V. Kamat, Chem. Rev. 93 (1993) 267.
[8] F.B. Li, X.Z. Li, M.F. Hou, Appl. Catal. B 48 (2004) 185.
[9] H. Park, W.Y. Choi, J. Phys. Chem. B 108 (2004) 4086.
[10] H. Liu, W. Yang, Y. Ma, Y. Cao, J. Yao, New J. Chem. 26 (2002) 975.
[11] J.G. Yu, J.C. Yu, W.K. Ho, Z.T. Jiang, New J. Chem. 26 (2002) 607.
[12] J.G. Yu, J.C. Yu, Chin. J. Chem. 21 (2003) 994.
[13] J.G. Yu, J.C. Yu, B. Cheng, X.J. Zhao, Sci. China B 46 (2003) 549.
[14] J.G. Yu, Y.R. Su, B. Cheng, M.H. Zhou, J. Mol. Catal. A 258 (2006) 104.
[15] J.G. Yu, G.H. Wang, B. Cheng, M.H. Zhou, Appl. Catal. B 69 (2007) 171.
[16] H. Kominami, M. Kohno, Y. Takada, M. Inoue, T. Inui, Y. Kera, Ind. Eng. Chem. Res. 38 (1999) 3925.
[17] Z.L. Wang, L.Q. Mao, J. Lin, J. Photochem. Photobiol. A 177 (2006) 261.
[18] H. Kominami, T. Matsuura, K. Iwai, B. Ohtani, S. Nishimoto, Y. Kera, Chem. Lett. 24 (1995) 693.
[19] H. Kominami, J. Kato, M. Kohno, Y. Kera, B. Ohtani, Chem. Lett. 25 (1996) 1051.
[20] H. Zhang, J.F. Banfield, J. Phys. Chem. B 104 (2000) 3481.
[21] J. Lin, J.C. Yu, D. Lo, S.K. Lam, J. Catal. 183 (1999) 368.
[22] J.G. Yu, J.C. Yu, B. Cheng, S.K. Hark, K. Iu, J. Solid State Chem. 174 (2003) 372.
[23] K.S.W. Sing, D.H. Everett, R.A.W. Haul, L. Moscou, R.A. Pierotti, J. Rouquerol, T. Siemieniewska, Pure Appl. Chem. 57 (1985) 603.
[24] J.C. Yu, J.G. Yu, J.C. Zhao, Appl. Catal. B 36 (2002) 31.
[25] M.E. Zorn, D.T. Tompkins, W.A. Zeltner, M.A. Anderson, Appl. Catal. B 23 (1999) 1.
[26] K.N.P. Kumar, J. Kumar, K. Keizer, J. Am. Ceram. Soc. 77 (1994) 1396.
[27] J.G. Yu, M.H. Zhou, B. Cheng, H.G. Yu, X.J. Zhao, J. Mol. Catal. A 227 (2005) 75.
[28] B. Karunagaran, D. Mangalaraj, K. Kim, B. Hong, Y. Roh, C.S. Park, J. Yi, Cryst. Res. Technol. 40 (2005) 222.
[29] T. Seikiya, S. Ohta, S. Kamei, M. Hanakama, S. Kurita, J. Phys. Chem. Solids 62 (2001) 717.
[30] W.K. Xu, S. Zhu, X.C. Fu, Q. Chen, Appl. Surf. Sci. 148 (1999) 253.
[31] B. Karunagaran, K. Kim, D. Mangalaraj, J. Yi, S. Velumani, Sol. Energy Mater. Sol. Cells 88 (2005) 199.
[32] B. Lindberg, R. Maripuu, K. Siegbahn, R. Larsson, C.G. Golander, J.C. Eriksson, J. Colloid Interface Sci. 95 (1983) 308.
[33] C. Yeongsoo, T. Umebayashi, M. Yoshikawa, J. Mater. Sci. 39 (2004) 1837.
[34] H. Kominami, J. Kato, S. Murakami, Y. Ishii, M. Kohno, K. Yabutani, T. Yamamoto, Y. Kera, M. Inoue, T. Inui, B. Ohtani, Catal. Today 84 (2003) 181.
[35] B. Ohtani, S. Nishimoto, J. Phys. Chem. 97 (1993) 920.
[36] J. Ovenstone, J. Mater. Sci. 36 (2001) 1325.
[37] M. Adachi, Y. Murata, I. Okada, S. Yoshikawa, J. Electrochem. Soc. 150 (2003) G488.
[38] J.T. Jiu, F.M. Wang, M. Adachi, Mater. Lett. 58 (2004) 3915.
[39] L. Wu, J.C. Yu, L.Z. Zhang, X.C. Wang, W.K. Ho, J. Solid State Chem. 177 (2004) 2584.
[40] Y. Sakatani, D. Grosso, L. Nicole, C. Boissiere, G. Soler-Illia, C. Sanchez, J. Mater. Chem. 16 (2006) 77.